Article:
Calautit, JK and Hughes, BR (2014) Wind tunnel and CFD study of the natural ventilation performance of a commercial multi-directional wind tower. Building and Environment, 80. 71 - 83. ISSN: 0360-1323

https://doi.org/10.1016/j.buildenv.2014.05.022

John Kaiser Calautit, Ben Richard Hughes, Wind tunnel and CFD study of the natural ventilation performance of a commercial multi-directional wind tower, Building and Environment, Volume 80, October 2014, Pages 71-83, ISSN 0360-1323, http://dx.doi.org/10.1016/j.buildenv.2014.05.022.

Wind tunnel and CFD study of the natural ventilation performance of a commercial multi-directional wind tower

John Kaiser Calautit – ***corresponding author***

School of Civil Engineering, University of Leeds, Leeds LS2 9JT, United Kingdom

Tel: +44 (0) 7544158981

Email: j.k.calautit@leeds.ac.uk

Ben Richard Hughes

School of Civil Engineering, University of Leeds, Leeds LS2 9JT, United Kingdom

Abstract

Scaled wind tunnel testing and Computational Fluid Dynamics (CFD) analysis were conducted to investigate the natural ventilation performance of a commercial multi-directional wind tower. The 1:10 scaled model of the wind tower was connected to the test room to investigate the velocity and pressure patterns inside the micro-climate. The tests were conducted at various uniform wind speeds in the range of 0.5 to 5 m/s and various incidence angles, ranging from 0˚ to 90˚. Extensive smoke visualisation experiments were conducted to further analyse the detailed airflow structure within the wind tower and also inside the test room. An accurate geometrical representation of the wind tunnel test set-up was recreated in the numerical modeling. Care was taken to generate a high-quality grid, specify consistent boundary conditions and compare the simulation results with detailed wind tunnel measurements. The results indicated that the wind tower was capable of providing the recommended supply rates at external wind speeds as low as 2 m/s for the considered test configuration. In order to examine the performance quantitatively, the indoor airflow rate, supply and extract rates, external airflow and pressure coefficients were also measured. The CFD simulations were generally in good agreement (0 – 20 %) with the wind tunnel measurements. Moreover, the smoke visualisation test showed the capability of CFD in replicating the air flow distribution inside the wind tower and also the test room.

Keywords: CFD; natural ventilation; rapid prototyping; wind tower; wind tunnel

Nomenclature

U	velocity magnitude (m/s)
X, Y, Z	Cartesian co-ordinates (m)
Re	Reynolds number
ρ	air density (kg/m^3)
v	kinematic viscosity (m^2/s)
Q	volume flow rate (m^3/s)
k	pressure loss coefficient
g	gravitational acceleration (m/s^2)
A	cross-sectional area (m^2)
ΔP	total pressure loss (Pa)
P	pressure (Pa)
P_o	total pressure (Pa)
P_s	static pressure (Pa)
L	length (m)
W	width (m)
H	height (m)

1. Introduction

In addition to electricity usage, buildings are also responsible for almost 40 % of the world's greenhouse gas emissions [1]. Space Heating, Ventilation and Air-conditioning (HVAC) represent the largest end use in buildings, accounting for almost two-thirds of the total energy use [2]. This signifies a major opportunity for reducing the energy consumption and greenhouse gas emissions. In recent years, natural ventilation techniques such as wind towers are increasingly being employed in new buildings for increasing the fresh air rates and reducing the energy consumption [3, 4]. Due to the increasing emphasis on using wind towers as natural ventilation technologies, there is constant scope for accurately analysing their performance in relation to external climates.

Wind towers were utilised in buildings in the Middle East for many centuries and their commercialisation has increased over the years [5, 6]. A wind tower is divided into quadrants, which allow fresh air to enter as well as stale (used) air to escape irrespective of the prevailing wind direction [7, 8]. There are two driving forces for the wind tower (Figure 1). The primary force provides fresh air driven by the positive air pressure on the wind-ward side, exhausting stale air with the assistance of the suction pressure on the leeward side. The secondary force is temperature driven where the density of air is less causing layers of air to be stacked.

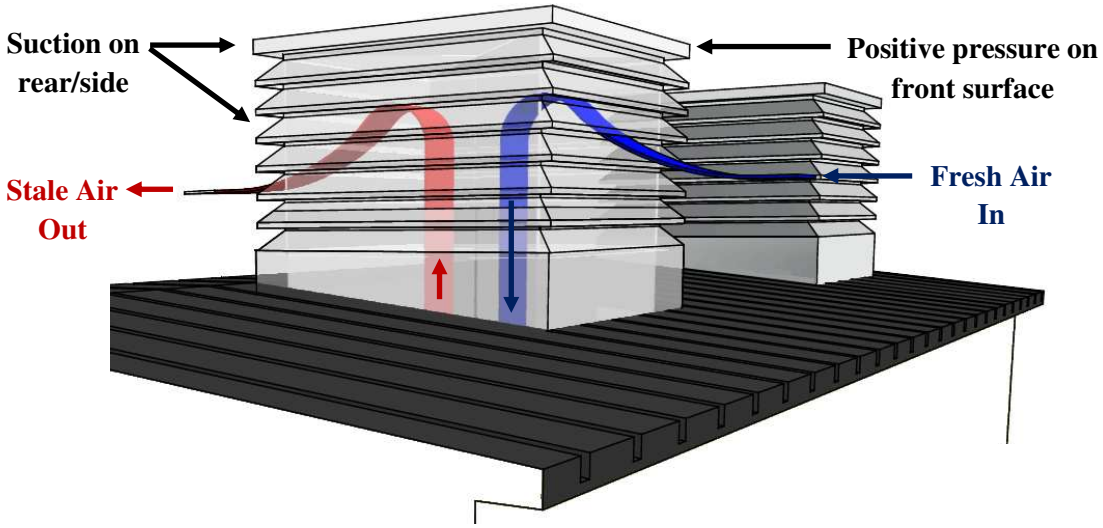

Figure 1 Flow diagram representing ventilation through a commercial wind tower device.

A number of studies [8, 9, 10] have assessed the ventilation performance of commercial wind towers using theoretical modelling. Elmualim [9] used mathematical equations proposed by BS5925:1991 for the performance analysis of a wind tower ventilation system. The mathematical equations were evaluated against experimental testing in a room in the building of School of Construction Management and Engineering, University of Reading in the UK. The wind tower was also evaluated against the use of a standard operable window with an equivalent opening area. The work concluded that the chosen ventilation design provided a substantially greater ventilation rate than an equivalent area of operable window. However, the results of the experimental testing showed the mathematical formula consistently overestimated the ventilation rate.

Later, an alternative semi-empirical approach was proposed by Jones and Kirby [8] in which a comprehensive theoretical model was coupled with experimental data to quantify the flow rates induced by a similar wind tower device. Included in the model were the effect of variations in wind speed and direction and the treatment of sealed and unsealed rooms. The semi-empirical model performed well against a range of CFD models [4, 11] and Elmualim's experimental data [9, 10], although this required certain assumptions about the wind direction. The authors concluded that developed model was the only practical approach to quickly and accurately estimate the wind tower performance. However, any error present in the experimental measurements will also appear in the theoretical model and so the accuracy of such model depends primarily on the available experimental data. Accordingly, there is a

need for a simple and reliable experimental methodology which can accurately estimate the wind tower performance under different wind conditions.

Although theoretical methods and laboratory experiments were usually employed in the study of natural ventilation devices, Computational Fluid Dynamics (CFD) modeling have recently been adopted in the study of airflow in buildings and have shown to be effective and advantageous in evaluating the performance of commercial wind towers. For example, Hughes and Ghani [11], Elmualim [12] and Liu *et al.* [4] all used CFD modeling to investigate the effect of the modification of the geometry components such as louvers and dampers on the ventilation rates. The wind tower CAD design in the CFD domain can be altered quickly and the remodeling done immediately. While, physical models requires more time and effort for design variations or adjustments.

Elmualim [12] studied the effect of volume control dampers and diffusers on the performance of a commercial wind tower using CFD modeling and experimental testing. Due to the size of the wind tower (1.5 m x 0.5 m), the experimental investigation was carried out in an open test section (2 x 2 m) wind tunnel as shown in Figure 2a. Clearly, the wind tower is nearly as large (in terms of height) as the test section opening, producing a blockage ratio of roughly 19 %. Additionally, variation of the velocity and temperature in the laboratory can also affect the simulated wind tunnel conditions since an open section was used. The study showed that the simulated wind profile was not fully uniform and was only relatively maintained around the louvers. A potential solution to this was to scale down the wind tower so it can fit inside the test section and ensure that the blockage ratio is small enough (less than 5 %) that the errors introduced are small and no corrections are required. This method was employed in the current research work.

The results showed that the damper and diffuser reduced the air flow by approximately 20 % at 3 m/s external wind velocity and 50 % at 1 m/s. The CFD code predicted a reasonable air flow rate compared with the wind tunnel result, despite the limitations of the wind tunnel test setup.

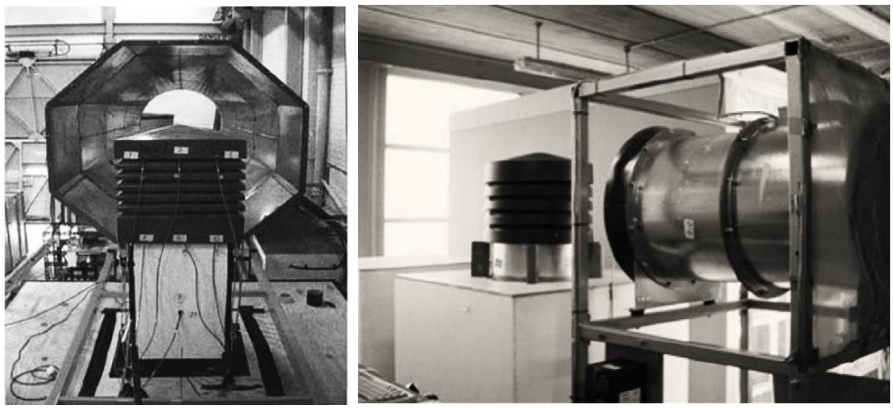

Figure 2 Existing experimental methods for the analysis of commercial wind towers: (a) open test section wind tunnel and (b) cone flow meter and blower fan method [10, 14].

A similar experimental method was employed in [9, 10] to validate the CFD predictions of the ventilation rates of a square wind tower. Hughes and Ghani [11] also investigated the effect of control dampers on the wind tower performance using CFD, validated with the experimental results of Elmualim [9, 10]. Although the wind towers were of different size the results were normalized for comparison purposes. Errors between the CFD results and experimental data were in the range of 0 – 30 %. Recently Liu *et al.* [4] evaluated the wind tower performance with different number of louvers and louver lengths using CFD. The work also focused on the analysing the indoor airflow patterns, apart from the effects of re-configuring the system. The study revealed that numerous works have investigated the effects of different configurations and components on the performance of the wind tower but only a few have investigated the internal conditions of rooms adopting the device.

The wind tower CFD results were validated against Elmualim's data [12] and good correlation was observed, although the numerical calculation domain in their CFD analysis did not accurately represent the experimental situation because an outdoor far field wind was considered instead of an open section wind tunnel. Since there was no experimental data available on indoor air flows supplied by commercial wind towers, the CFD modeling of the air flow pattern inside the room was validated against the findings of a displacement ventilation experiment conducted by Chen and Srebric [13]. The present study addresses this by providing a detailed CFD-wind tunnel analysis of the indoor air flow.

To this end, Su *et al*. [14] evaluated the flow rate supplied by a commercial wind tower using a measurement system which included a cone flow meter and blower fan as shown in Figure 2b, this approach was similar to the method used by Elmualim [12]. The measured data was compared with CFD results, and a good agreement between two methods has been achieved.

This was expected, as the CFD domain was modeled to accurately represent the experimental situation. Furthermore, CFD modelling of the wind tower was carried out to create the conditions similar to the situation of outdoor far field wind. The work concluded that the CFD modelling results were quite different between the situation of a blower fan and outdoor wind. The calculated extract flow rate of the wind tower in a far field wind was approximately double that for the situation using a blower fan.

A few studies have also used a CFD-wind tunnel methodology in predicting indoor airflows. Lo *et al*. [29] used wind tunnel testing coupled with CFD for indoor airflow prediction of wind-induced cross ventilation. The wind tunnel measurements and weather data were used as inputs for the CFD boundary conditions. The work included the effect of wind fluctuations, such as change in wind velocities and angles. The results showed that it is possible for the suggested method to accurately predict the average cross ventilation through small openings. Tecle *et al*. [30] used a boundary layer wind tunnel to study the wind-driven natural ventilation for a low-rise building at a model testing scale of 1:20. The effects of size of openings, room partitioning, inlet-outlet ratio, screens on the pressure drops and inlet discharge coefficient were evaluated.

This paper presents a fully validated methodology for the investigation of the ventilation performance of a commercial wind tower. An accurate geometrical representation of the experimental situation was recreated in the CFD simulation. Care was taken to generate a high-quality grid, specify consistent boundary conditions and compare the simulation results with detailed wind tunnel measurements. The work used rapid prototyping to allow the accurate modeling of the complex components of the wind tower device at a much smaller scale (1:10). The investigation was conducted in a closed-loop low speed wind tunnel specifically designed for the experimental testing of natural ventilation devices. The approach will provide a solution to the current limitations of the experimental testing of commercial wind towers found in the review of previous works.

2. CFD method

The basic assumptions for the CFD simulation include a three-dimensional, fully turbulent, and incompressible flow. The internal and external flow was modeled by using the standard k–epsilon turbulence model. This technique is well established in the field of natural ventilation research [3-15]. The CFD code used the Finite Volume Method (FVM) approach and employed the Semi-Implicit Method for Pressure-Linked Equations (SIMPLE) velocity-

pressure coupling algorithm with the second order upwind discretisation as suggested in the literature [3-15]. The governing equations will not be repeated here but are available in [16].

The CFD analysis was carried out using the ANSYS 12.1 Fluent software. A flow domain representation of the physical geometry of the wind tower design under investigation is shown in Figure 3a. The macro-climate with the height, width, and length of 5, 5, and 10 m was created to simulate the external wind velocity. Furthermore, the wind tower system was incorporated to a test room (micro climate) with the height, width, and length of 3, 5, and 5 m representing a small classroom of 15 people [17, 18].

2.1 Mesh generation

The accuracy of the results achieved from the CFD modeling is highly dependent on the quality of the mesh, which equally have implications on the convergence of the model [19, 20]. A non-uniform mesh was applied to the entire computational model. The mesh arrangement consisted of 4,045,896 hybrid non-uniform mesh elements. The generated computational mesh of the wind tower and test room model are shown in Figure 3b.

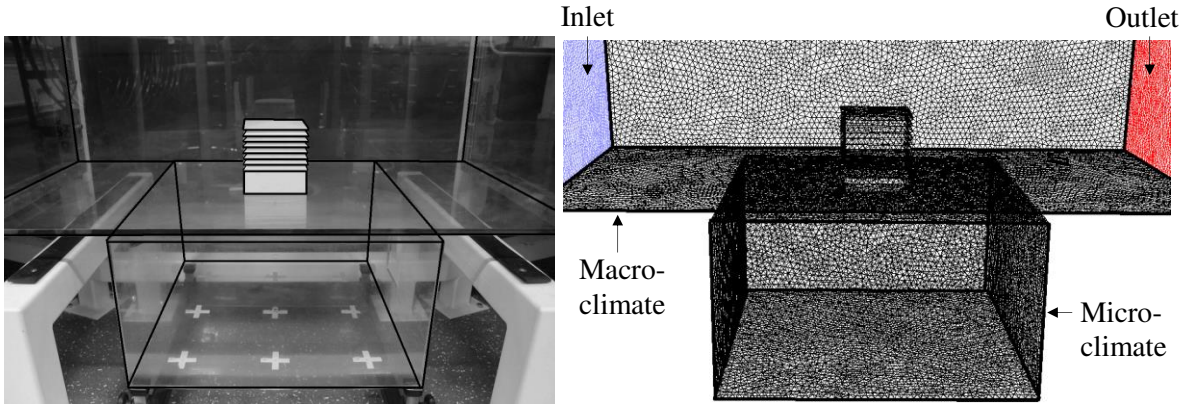

Figure 3 (a) Wind tower model inside the wind tunnel test section (b) view of the computational mesh of the wind tower model and test room

The grid was modified and refined around critical areas of interests in the simulation. The size of the mesh element was extended smoothly to resolve the sections with high gradient mesh and to improve the accuracy of the results of the velocity fields. Inflation parameters were set for the complex geometry face elements to generate a finely resolved mesh normal to the wall and coarse parallel to it. The two-dimensional face elements at the selected wall or boundaries were inflated into 3D prism elements which resolved the boundary layer properly at relatively less computational cost [21].

Grid sensitivity analysis was used to validate the programming and computational operation of the computational model. The numerical grid was refined and locally enriched using the hp-method grid adaptation technique [19, 22]. The grid was evaluated and refined (mesh sizes ranging from 1,622,108 to 7,149,235 elements) until the posterior estimate error becomes insignificant between the number of nodes and elements, computational iterations and the posterior error indicator. The maximum error for the average velocity was 4.38 %. The discretization error was found to be the lowest at over 7 million cells for the indicated variable. The applied boundary conditions were kept constant throughout the simulation process to ascertain precise comparison of the posterior error estimate.

2.2 Boundary conditions

Figure 3 shows the physical domain containing the macro-climate and micro-climate fluid volumes. A wall boundary condition was used to create a boundary between each region. The macro-climate fluid volume, used to simulate the external velocity flow field, generates a velocity into the wind tower. To generate a velocity flow field one horizontal plane was named as a velocity inlet, with the opposite boundary wall set as pressure outlet. Boundary conditions for the numerical modeling of the flow were chosen to be the same as the conditions in the wind tunnel during the experiment. A uniform velocity inlet profile was used. The boundary conditions for the CFD model are summarised in Table 1.

Table 1 Summary of the CFD model boundary conditions.

Time	Steady State
Velocity inlet (m/s)	0.5 – 5 [23]
Wind angle (˚)	0 - 90
Pressure outlet	Atmospheric [23]
Gravity	-9.81
Walls	All walls: no slip [23]
Roughness height K_S (10^{-3} m)	Macro-micro climate walls: 0.001 [23]
Roughness constant C_{KS}	All walls: 0.5 [23]

3. Experimental method

A 1:10 scaled model of a commercial multi-directional wind tower was used in the experimental study. The investigation was conducted in a closed-loop low speed wind tunnel in the Building Physics Laboratory of the School of Civil Engineering of the University of Leeds [23]. The wind tunnel has an overall plan length of 5.6 m with a test section of the height, width, and length of 0.5, 0.5, and 1 m (Figure 4). The tunnel operates as closed circuit, air that passes through the test section is drawn back into the fan and recirculated into

the test section repeatedly. Guide vanes were used to turn the air flow around the corners of the wind tunnel. According to the dimensions of the 1:10 model and the wind tunnel cross-section, the wind tower scaled model produced a maximum wind tunnel blockage of 4.8% (0.2 m from side walls and 0.4 m from top wal of the test section l), and no corrections were made to the measurements obtained with these configurations [5, 23]. Additionaly, the distance of the wind tower model from the inlet and outlet of the test section was 0.4 m.

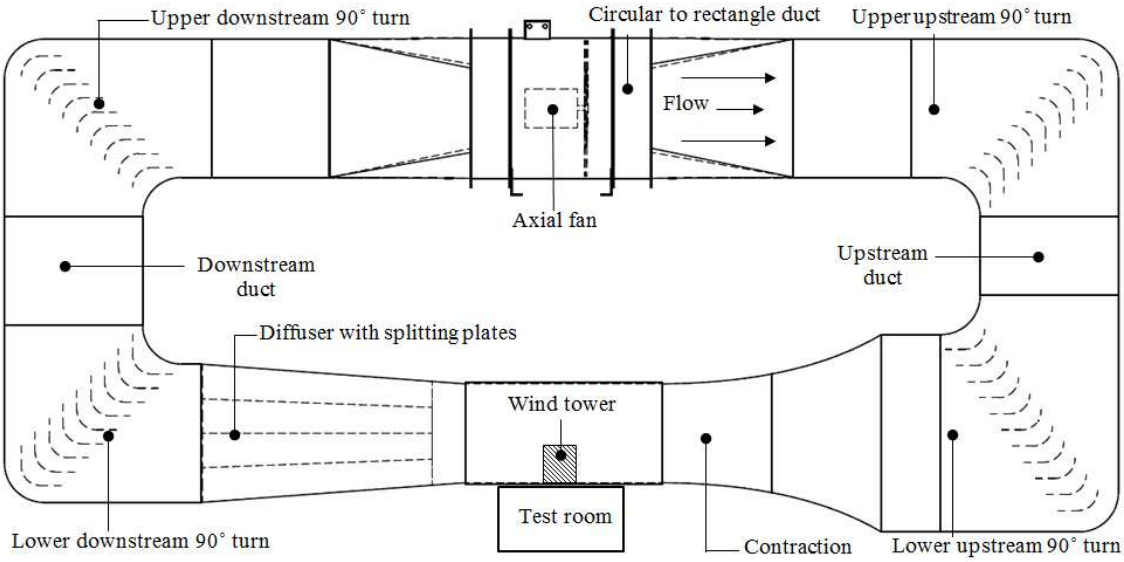

Figure 4 Side view of the closed-loop low speed wind tunnel facility for investigating the natural ventilation performance of the wind tower device

Wind tunnel testing on scaled models should ideally be simulated at the same Reynolds number as would be experience by the full scale model, thus satisfying the Reynolds number similarity. Strict scaling of wind and turbulence Reynolds number for the simulated flow is generally not possible for wind tunnel model testing of building and structures, even in the largest, high speed and most expensive wind tunnels [4]. However, the equality of model and full-scale Reynolds number, based on the mean wind speed and a characteristic dimensions of the structure, is not necessaary for sharp edged structure, provided that the model Reynolds number is not less than 10,000 [24]. The flow separation points are fixed at these sharp corner location regardless of Reynolds number, so that wind responses tends to be less sensitive to Reynolds number. Geometric similarity of model was achieved by equally scaling down the relevant dimensions of the wind tower model and test room by the appropriate factor [26]. One of the main objective of this work was to present a fully validated CFD-scaled wind tunnel methodology. Therefore it was ensured that the conditions simulated in the CFD was exactly the same as in the wind tunnel test section. Due to the limitations of the experimental

setup, the effect of the atmospheric boundary layer on the ventilation performance was not investigated in the study.

3.1 The wind tower and test room model

The creation of an accurate scaled wind tunnel prototype was essential for the experimental study. The wind tower geometry features a variety of unconventional and complex parts such as the external louvers, cross-dividers and top hat. Therefore the wind tunnel model was constructed using rapid prototyping and three dimensional computer aided design (CAD) data. Furthermore, 3D prototyping makes it possible to easily embed equipment into the model such as pressure measurement devices. Figure 5 shows the 3D printed 1:10 multi-directional wind tower scale model design.

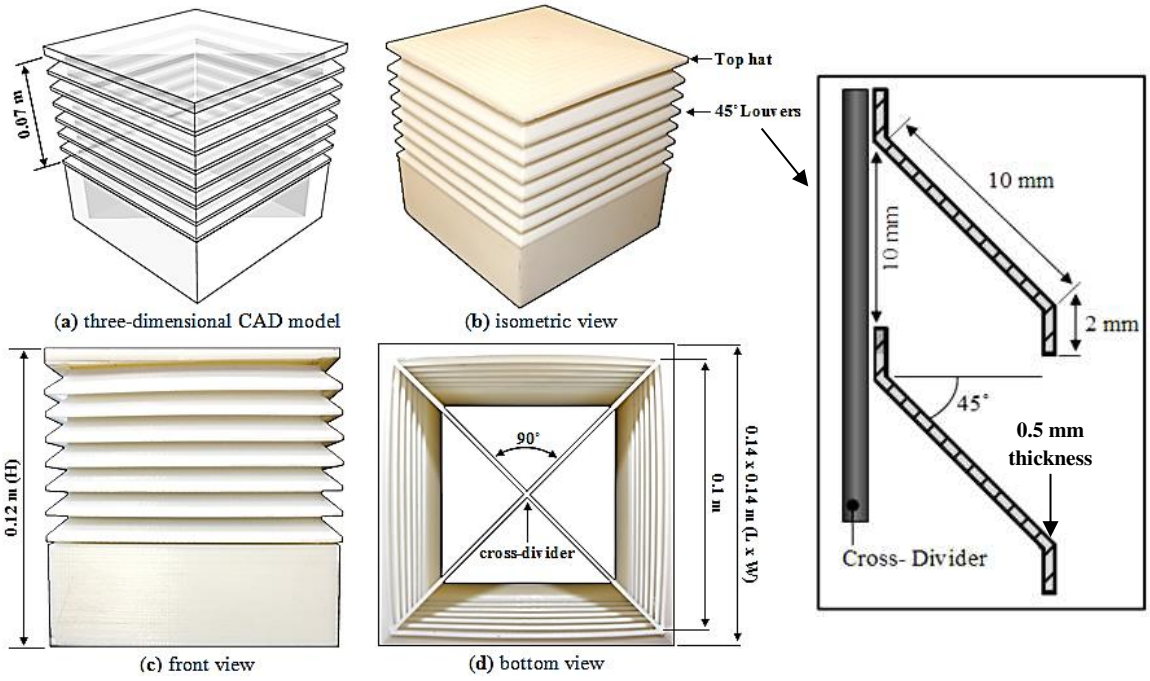

Figure 5 A 1:10 three-dimensional CAD model of the multi-directional wind tower (a) and the resulting 3D prototype model (b, c and d) built using the 3D printer.

The wind tower model was connected to a 0.5 x 0.5 x 0.3 m test room (representing the ventilated space), which was mounted underneath the wind tunnel test section. The test room model was made of acrylic perspex sheet to facilitate flow visualisation testing as well as to be able to clearly see the measurement points markers. The test room top plate was constructed so that it could be rotated in the test section in order to test different approaching wind directions (0 to 90˚). In order to measure the velocity inside the room at the points

using the hot-wire anemometer, a total of 14 openings were created across the front and side walls of the test room.

3.2 Experimental set-up and measurement procedures

3.2.1 Indoor airflow distribution

In this study the airflow inside the test room model was measured using a hot-wire anemometer. Hot-wire anemometers have been used extensively in wind tunnel experiments over several decades. The measurement technique relies on electrically heating a thin wire or foil which is then cooled by the flow of air. The cooling rate is thus related to the wind speed. Furthermore, hot-wire anemometers are sensitive to very small internal velocities, which were present during the investigation. Nine data points in an equally spaced 3 by 3 grid were created within the test room at a height of 1.5 m which allow for measurements to be made for velocity within the test room (Figure 6). Additionally, three data points were positioned at the bottom of the room (central), below the supply and exhaust channels of the wind towers. The values of the velocity were obtained from the three components of the vector (X, Y, and Z). The tests were carried out between velocities ranging from 3 m/s and 5 m/s. The flow in the wind tunnel was allowed to normalise before measurements were taken.

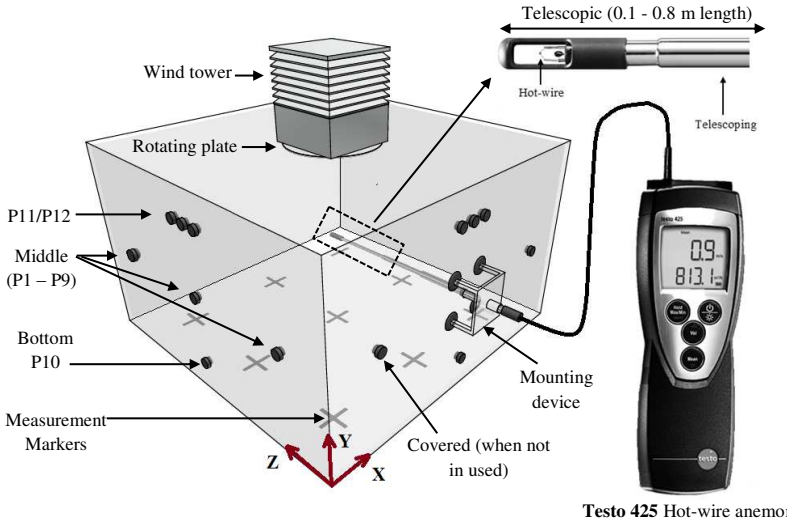

Testo 425 Hot-wire anemometer

Measurement Points

Point	*X* [m]	*Y* [m]	*Z* [m]
P1 (mid)	-0.165	-0.135	0.165
P2 (mid)	0	-0.135	0.165
P3 (mid)	0.165	-0.135	0.165
P4 (mid)	-0.165	-0.135	0
P5 (mid)	0	-0.135	0
P6 (mid)	0.165	-0.135	0
P7 (mid)	-0.165	-0.135	-0.165
P8 (mid)	0	-0.135	-0.165
P9 (mid)	0.165	-0.135	-0.165
P10 (bottom)	0	-0.22	0
P11 (supply)	0.025	-0.03	0
P12 (outlet)	-0.025	-0.03	0

Figure 6 Test room experimental setup and measurement points.

The hot wire probe (Testo 425) gave velocity measurements with an uncertainty of $\pm$1.0 % rdg. at speeds lower than 8 m/s and uncertainty of $\pm$ 0.5 % rdg. at higher speeds (8 – 20 m/s).

3.2.2 Volumetric flow supply rate

The induced airflow into the test room was measured using the hot wire anemometer positioned below the channels of the wind tower device (Figure 6). The cross-sectional area of the wind tower channel was divided into several portions and the airflow rate through it was calculated as follows:

$$Q = \sum_{i=1}^{n} A_i \times U_i \qquad \text{Equation 1}$$

Figure 7 shows the location of the points inside the channel quadrants at a height of 0.27 m from the test room floor. The tests were carried out at various wind angles (0 - 90˚).

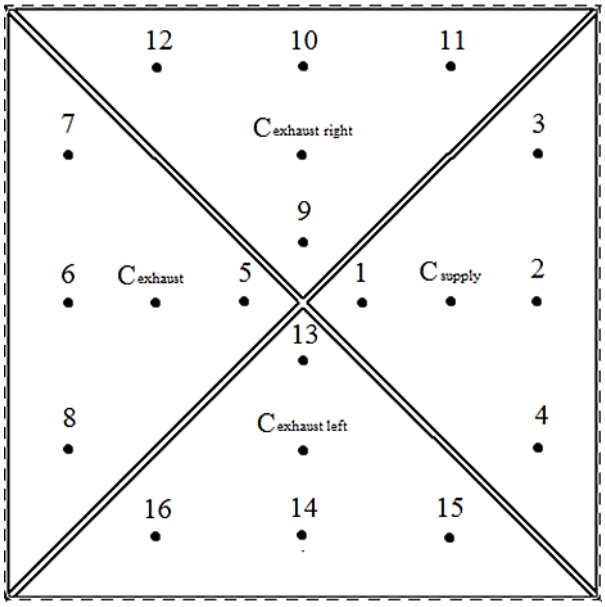

Point-i	*X* [m]	*Y* [m]	*Z* [m]
1	0.050	0.060	0.270
2	0.005	0.090	0.270
3	0.075	0.090	0.270
4	0.025	0.090	0.270
C_{supply}	0.050	0.075	0.270
5	0.050	0.040	0.270
6	0.050	0.010	0.270
7	0.075	0.010	0.270
8	0.025	0.010	0.270
$C_{exhaust}$	0.060	0.050	0.270
9	0.060	0.050	0.270
10	0.090	0.050	0.270
11	0.090	0.075	0.270
12	0.009	0.025	0.270
$C_{exhaust\ left}$	0.075	0.050	0.270
13	0.040	0.050	0.270
14	0.010	0.050	0.270
15	0.010	0.075	0.270
16	0.010	0.025	0.270
$C_{exhaust\ right}$	0.025	0.050	0.270

Figure 7 Section view of the wind tower supply and exhausts channels showing the location of the measurement points.

3.2.3 External airflow measurement

The velocity of the airflow around the wind tower model was also measured using the hot-wire anemometer (Table 2). The purpose of this test was to evaluate the accuracy of simulating or achieving the flow characteristics around the wind tower model. The values of the velocity

Table 2 Summary of the measurement coordinates inside the wind tunnel test section.

Point	*X* [m]	*Y* [m]	*Z* [m]
A	0.250	0.250	0.110
B	0.425	0.300	0.110
C	0.425	0.250	0.110
D	0.425	0.200	0.110
E	0.500	0.330	0.110
F	0.425	0.250	0.055
G	0.575	0.250	0.110

3.2.4 Pressure coefficients

The pressure measurements were referred to the upstream dynamic pressure using the reference velocity in the test section in the case of a uniform wind flow. The air pressure coefficient C_p was calculated using the following equation [5]:

$$C_p = \frac{p - p_s}{\frac{1}{2}\rho U_{ref}^2} \qquad \text{Equation 2}$$

The model was fitted with 15 pressure taps located inside the model (Figure 8). The reference velocity, static and dynamic pressure were monitored using the pitot-static tubes mounted above the wind tower model. The uncertainties associated with the pressure readings (DPM ST650 with the 166T ellipsoidal Pitot-static tubes) were estimated to be $\pm$ 1.0 % of reading at 22˚C. The valid angle range for the pitot - static tube calibration was within the range of $\pm$ 11˚.

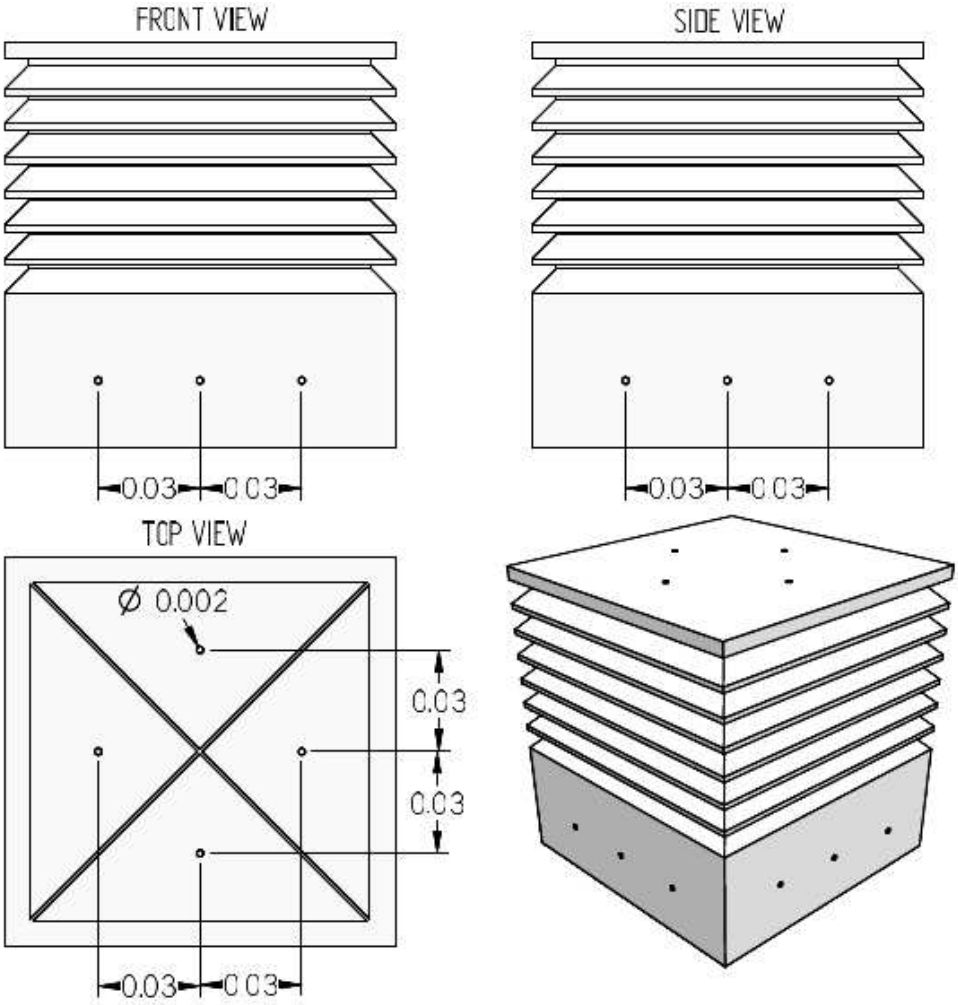

Figure 8 Pressure tap locations and dimensions

The surface pressure was transmitted to a Scanivalve digital pressure transducer, a sixteen channel DSA3217 digital sensor array, through the 0.0016 m outside diameter tubulations. The unit contains a 16 bit A/D converter and it communicates data to DSAlink3 via Ethernet connection. The data was acquired at a sampling rate of 1000 samples/sec. For each pressure tap, 5 records of the pressure data, each comprising of 1,000 data points was acquired.

3.2.5 Flow visualisation

In order to recognise the flow pattern in and around the wind tower model, smoke visualisation tests were also carried out. The tests were conducted in the uniform flow wind tunnel at various wind angles (0 – 90˚). Figure 9 shows the smoke visualisation test setup in the test section.

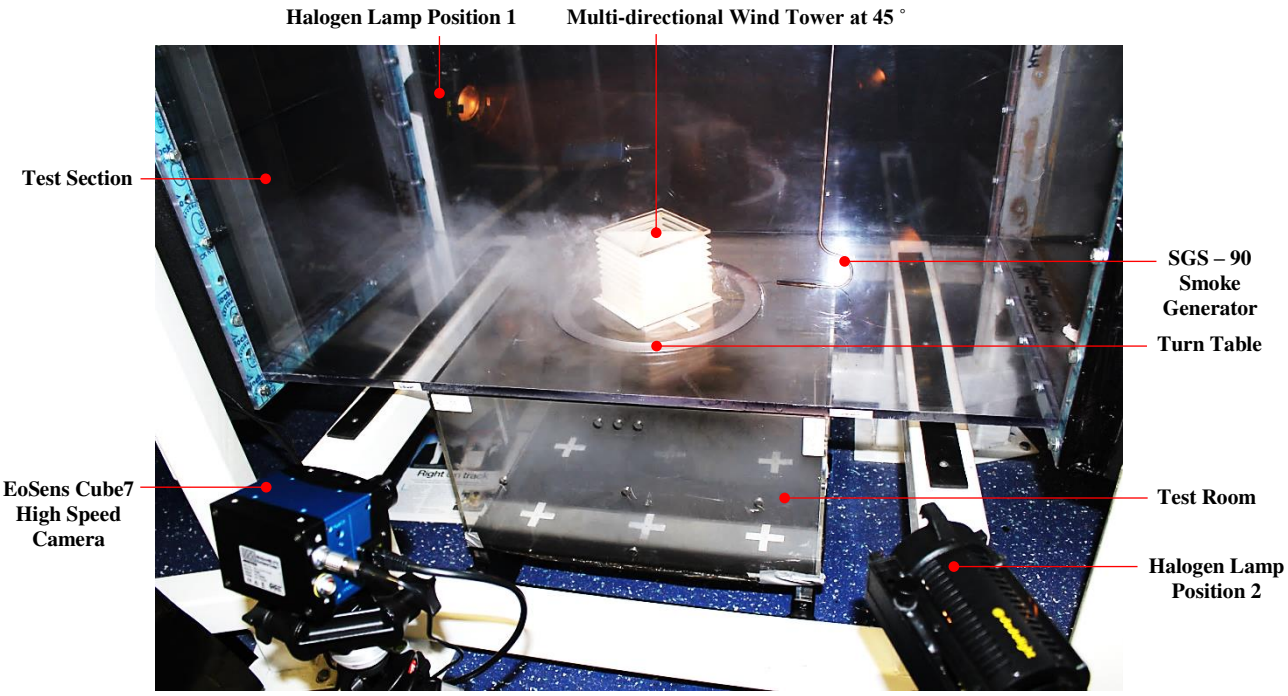

Figure 9 Wind tunnel smoke visualisation set-up.

The model was exposed to a free stream air velocity of 3 m/s to obtain smoke of a sufficiently high concentration. The experimental flow visualisation also helped to identify the supply and extract segments during all tests.

4. Results and Discussion

4.1 CFD Results

4.1.1 Overall airflow distribution

Figure 10 shows the velocity contour plot through the centre of the model to assist the illustrative analysis. From the plot, the air flow enters the inlet boundary velocity on the right and the flow splits with some of the air entering the wind tower and some passing over or shearing and exiting to the pressure outlet on the left. The flow entering the wind tower accelerates as it enters the device reaching maximum velocity of 2.8 m/s as it hits the cross-dividers and forces the flow down into the diffuser. At an inlet velocity of 3 m/s, the average velocity exiting the wind tower diffuser was 1.62 m/s while the average velocity in the microclimate was obtained at 0.55 m/s. Minor air short-circuiting was observed below the wind tower channel.

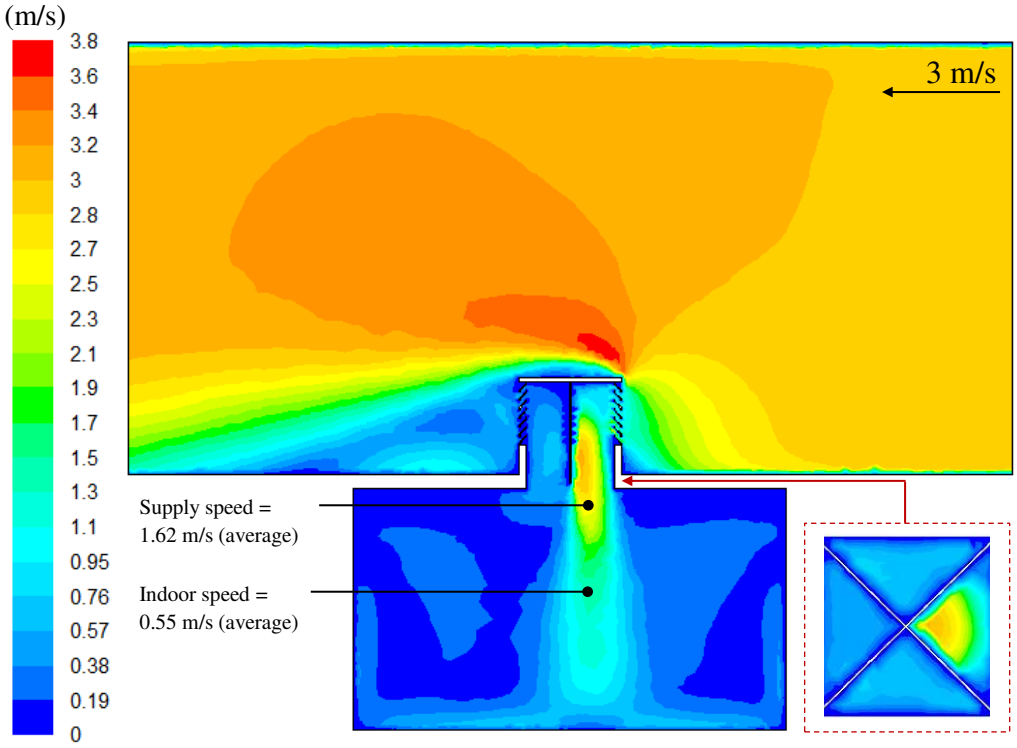

Figure 10 CFD velocity contour plot of a cross sectional plane in the test room with an inlet velocity of 3 m/s.

4.1.2 Overall pressure distribution

Figure 11 displays the static pressure contour of the cross-sectional plane inside the test room. The highest pressure (red area) was obtained at the upstream of the louvers with a maximum value of 5.8 Pa. Negative pressure (blue area) was observed at the exit and upper side of the wind tower with a minimum value of -6.6 Pa. The average pressure inside the microclimate was -1.28 Pa. The room under negative pressure indicates that less air is supplied to the room than exhausted which was the case for the multi-directional wind tower at 0˚ angle; there are three exhaust quadrants and only one supply quadrant.

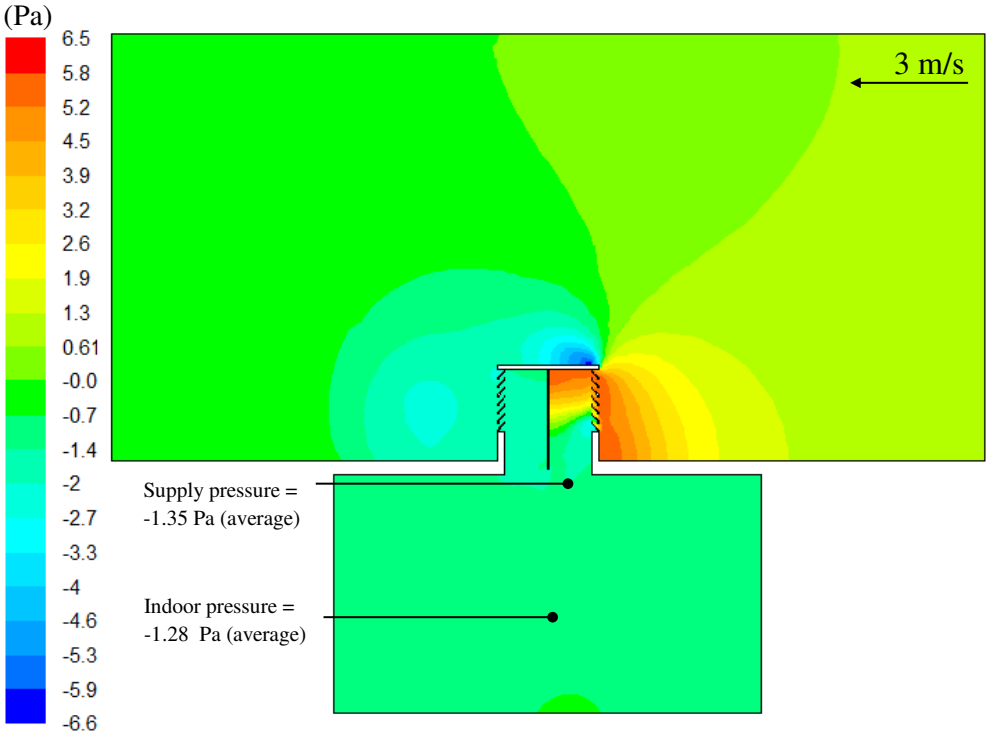

Figure 11 CFD static pressure contour plot of a cross sectional plane in the test room with an inlet velocity of 3 m/s.

4.1.3 Volumetric airflow rate

Different incident wind angles were investigated to examine the effect on the overall performance of the multi-directional wind tower model. 5 different models (0, 30, 45, 60, 90˚) were generated and solved at an external wind speed of 3 m/s. Figure 12 shows the CFD results of the volumetric airflow through the wind tower quadrant at different wind angles. In this figure the supply and the extract segments are recognised by positive and negative values of airflow rate. A volumetric airflow rate of 0.32 m^3/s was achieved through the supply quadrant 1 at 0° for an average wind speed of 3 m/s. As the wind angle increases the supply airflow through quadrant 1 decreases. Exceeding the wind angle over the transition angle (> 70°), caused a change in airflow direction into quadrant 1. At 45° wind angle, a net volumetric flow rate of 0.47 m^3/s was achieved through the combined supply quadrants 1 and 3 with the exhaust flow rate from the opposite quadrants at its maximum.

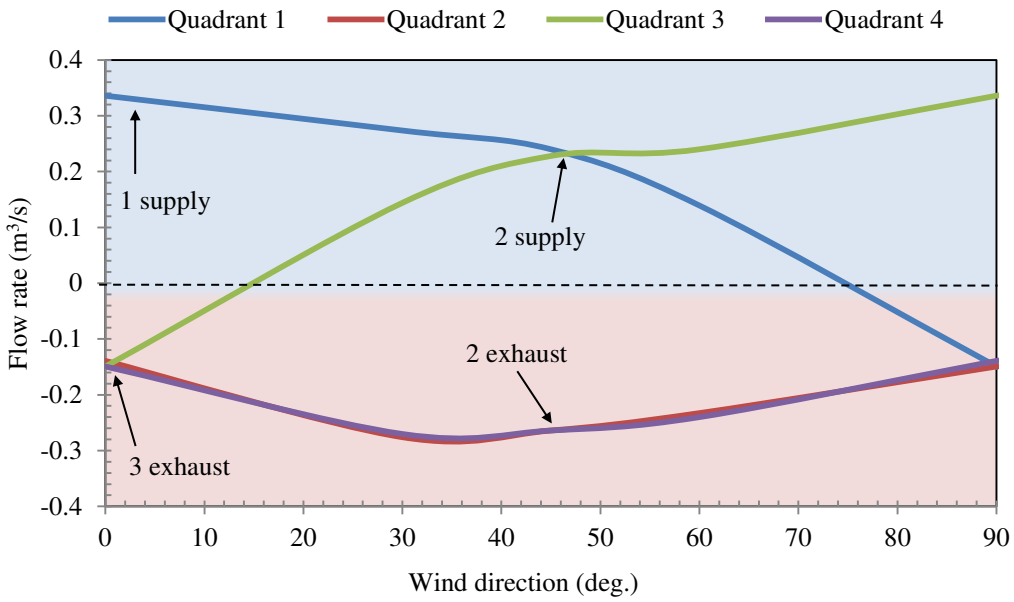

Figure 12 Volumetric airflow through the wind tower quadrants for different wind directions.

41.4 CFD results summary

The simulation models were tested for varying wind speeds (0.5 m/s – 5 m/s). The supply rates (diffuser), indoor velocity and static pressure readings were taken from the weighted-average value at the diffuser surface (Figure 7) and indoor points (Figure 6). The results for the simulations are summarised in Table 4. Building Regulations suggests that a minimum air supply rate per occupant of 10 L/s per occupant [27] is required for a small classroom of 15 people [17]. The wind tower does not meet this recommendation for an external wind velocity of 1 m/s and below; however, the system surpasses the recommendation exponentially as the external velocity increases (2 m/s and above) as shown in Table 3.

Table 3 Simulation results for the commercial multi-directional wind tower.

Inlet speed [m/s]	CFD supply rate [L/s]	CFD supply rate [L/s/occupant] *15 occupants*	Building Regulation 2000 [L/s/occupant] *15 occupants*	CFD [L/s/m^2] *Area = 25 m^2*	Average indoor velocity [m/s]	Average indoor pressure [Pa]
0.50	62.50	**4.17**	**10.00**	2.50	0.09	-0.05
1.00	135.00	**9.00**	**10.00**	5.40	0.19	-0.12
2.00	275.00	18.33	10.00	11.00	0.40	-0.61
3.00	405.00	27.00	10.00	16.20	0.55	-1.28
4.00	575.00	38.33	10.00	23.00	0.81	-2.41
5.00	722.50	48.17	10.00	28.90	0.99	-3.64

4.2 Experimental validation

4.2.1 Indoor airflow distribution

Figure 13 displays the velocity contour plot (top view, height = 0.15 m) of a cross-sectional plane inside the microclimate. As expected, maximum velocity was achieved at the centre of the room with a maximum value of 1.4 m/s. A uniform trend was achieved across the sides of the domain as the velocity decreased to an average value of 0.44 m/s across the remaining vertices. The graph shows a comparison between the experimental and CFD results for the velocity measurements. It was observed that the CFD slightly over or underestimated the airflow speeds at the measurement points. The trend (points 1 - 12) shows that the CFD model was capable of predicting the airflow inside the test room. The average error across the points was measured at 9 %. Using a similar justification as recommended in [27] it was claimed that the validation of the CFD modelling study was acceptable.

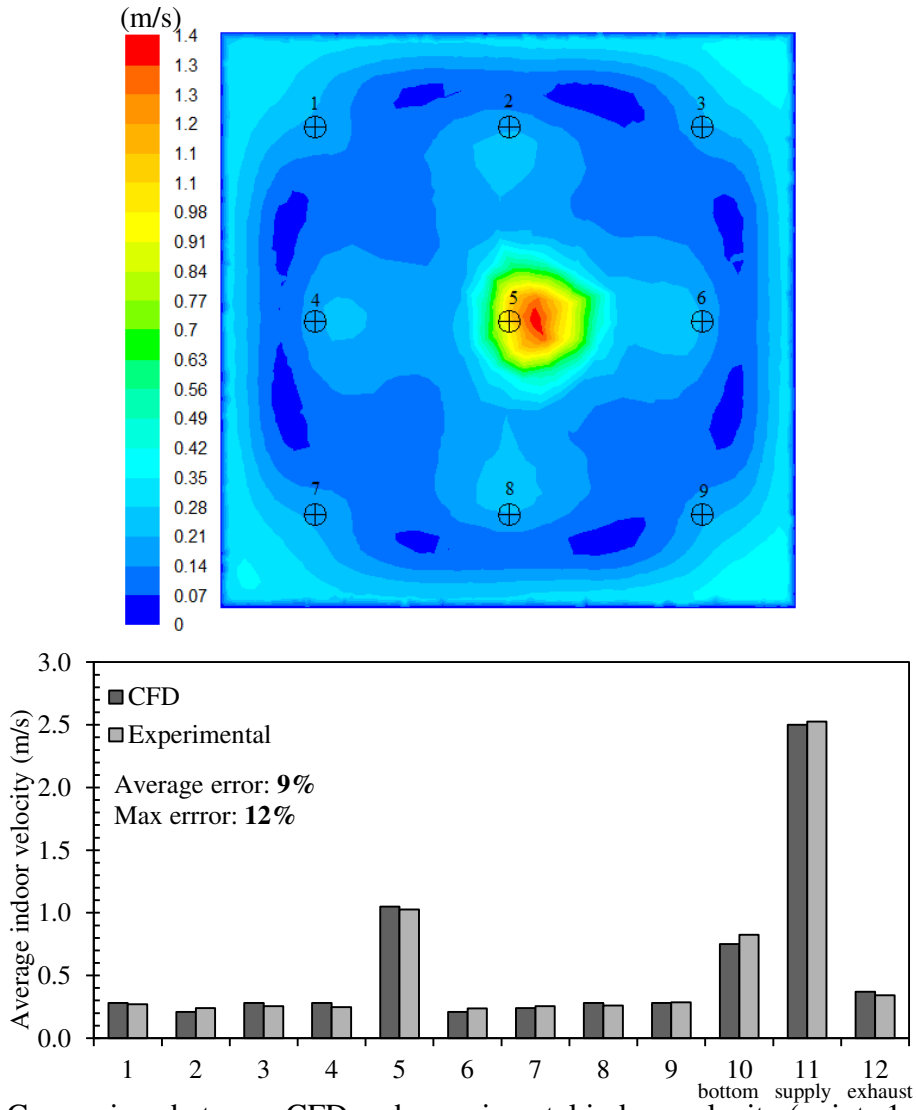

Figure 13 Comparison between CFD and experimental indoor velocity (points 1 – 12) with external wind speed at 3 m/s.

4.2.2 Supply and exhaust airflow measurement

Figure 14 displays the velocity contours inside the wind tower channel. Maximum velocity was achieved at the windward quadrant with a maximum value of 3.1 m/s. The graph shows a comparison between the experimental and CFD results for the velocity measurements. A good agreement was observed between both methods of analysis with the error less than 10 % for all points except for point 6 which was located at the exhaust quadrant. Average error across the points was 8.6 %. Using a similar justification as recommended in [27] it was claimed that the validation of the CFD modelling study was acceptable.

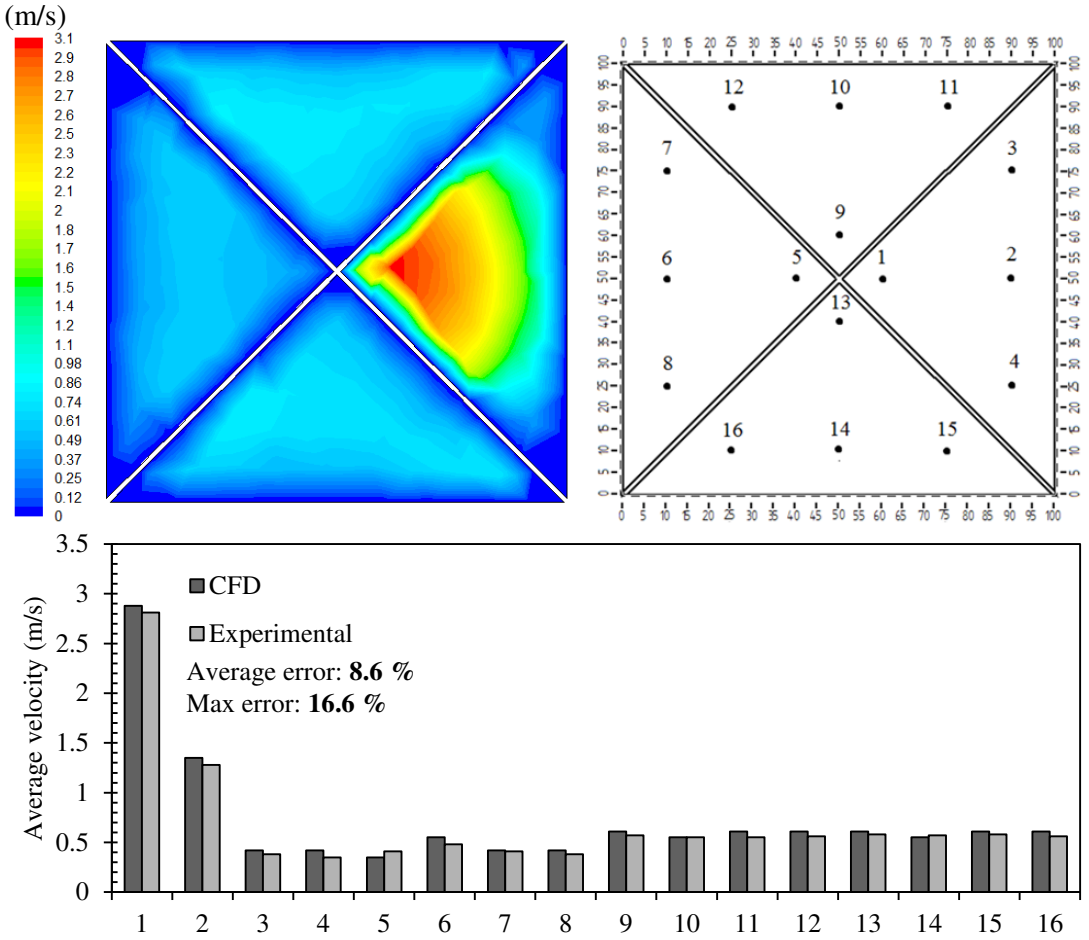

Figure 14 Comparison between CFD and experimental results for the velocity in the supply and exhaust channels with external wind speed at 3 m/s.

4.2.3 External airflow measurements

Table 4 shows the comparison between the measured and CFD values for the dimensionless velocity X, Y and Z for points A – G around the wind tower model. The flow speed values were made dimensionless by dividing its value by a reference wind speed, which was the measured speed at point A (mean). A good agreement was seen between both methods of

analysis with the error less than 10 % for all velocity components for all points except for point G (x – velocity component), which was located at the wake region of the airflow around the wind tower. This was one of the known limitations of the k-epsilon turbulence model; not performing well for complex flows such as severe pressure gradients and large flow separations. The average error percentage across all the measurement points was 8 %.

Table 4 Comparison between measured and CFD results for mean velocity at points A - G (X, Y, Z) (stream wise, vertical and lateral) around the wind tower model.

Points	z x y	U_X actual dimensionless	U_Y actual dimensionless	U_Z actual dimensionless	U_X CFD dimensionless	U_Y CFD dimensionless	U_Z CFD dimensionless
A	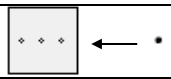	**1.000**	0.063	0.035	**1.000**	0.065	0.032
B	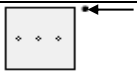	0.850	0.366	0.384	0.848	0.372	0.394
C	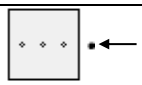	0.689	0.415	-0.025	0.653	0.430	-0.025
D	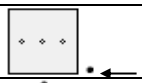	0.884	0.363	0.380	0.841	0.372	0.386
E	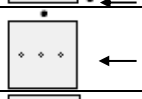	0.918	-	-	0.884	-	-
F	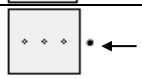	0.468	0.181	-0.004	0.465	0.181	-0.004
G	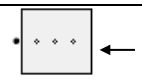	0.255	0.120	-0.078	0.218	0.116	-0.087

4.2.4 Surface pressure coefficient

Figure 15 shows the measured and CFD values for the pressure coefficients at the front, back, left, right and top surfaces of the wind tower model. As expected the points located at the front surface experienced the maximum value, and with the moving air stream towards the top, right and left side, the pressure coefficient decreases, indicating the acceleration of the flow. The measured pressure coefficients along the right and left surfaces of the wind tower were similar, indicating the flow regularity for the zero incident angle wind. The pressure coefficient dropped sharply across the Point P1 – Top. This point was at the front edge of the top surface where flow separation occurs. While for the back side of the of the wind tower model, a uniform pressure distribution was observed. This was due to the separation of the air stream from the sides; an almost uniform low pressure wake was formed around the back surface. CFD and experimental results indicated a good correlation, with the error below 10 % except for point P2 – top and back. Measurements at the front surface of the wind tower

gave the highest accuracy with average error of only 5 % between the points. Errors in wind tunnel pressure measurements are typically about 10 - 20 % [28] which suggests that the discrepancy between the CFD and experimental results were due predominantly to errors in the CFD predictions, rather than errors in the measured results.

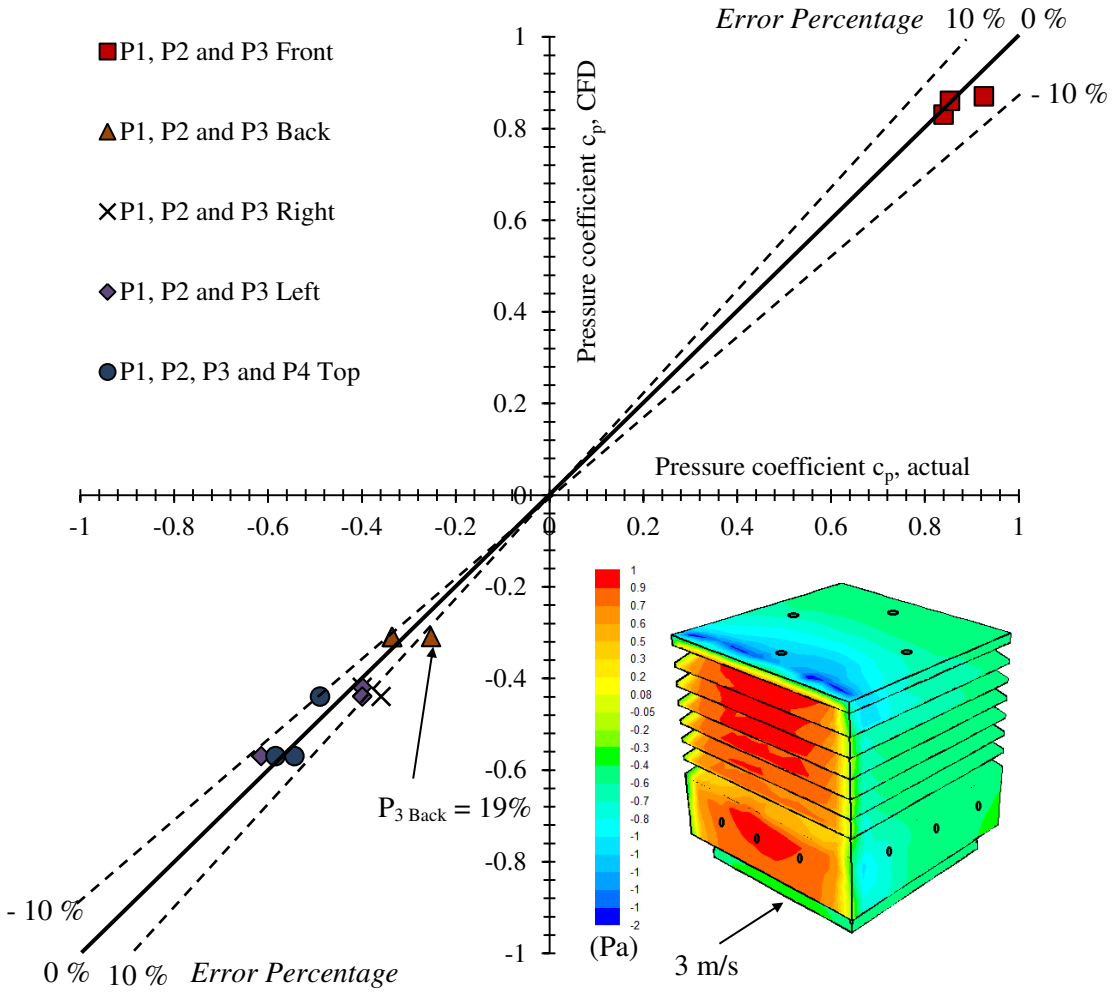

Figure 15 Comparison between CFD and experimental values for surface pressure coefficients around the wind tower model. Dotted lines represent 10 % error percentage.

4.2.5 Flow visualisation

In order to recognise the flow pattern in and around the wind tower model, smoke visualisation tests were also carried out. The tests were carried conducted in the uniform flow wind tunnel at various wind angles (0 - 90˚). Figure 16 and Video 1 shows the predicted and visualised flow pattern inside the test room model, the flow smoothly passes around and over the wind tower with some of the air entering the wind tower supply channel through the 45˚ louvers. Higher velocity at the point of entry was more visible due to the amount of smoke being displaced at this side of the wind tower. The airflow was directed towards the floor of

the test section and spread outwards in all directions. As the airflow hits the bottom surface the air slows down and flows through the side walls, with some of the air escaping through the exhaust quadrant of the wind tower which was at a lower air pressure. It was also observed that some of the air entering through the supply quadrant was immediately leaving through the exhaust without flowing inside the test room (small short circuiting). In Video 1 the air short circuiting effect can be observed at 00:04. A region of highly recirculating flow was seen immediately at the downstream of the wind tower.

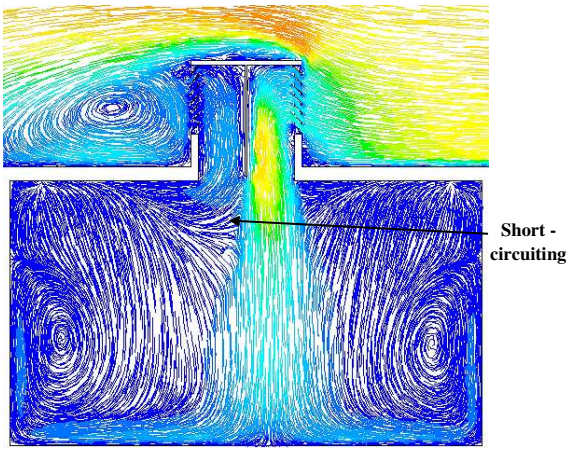

Figure 16 CFD streamlines inside the test room with the multi-directional wind tower.

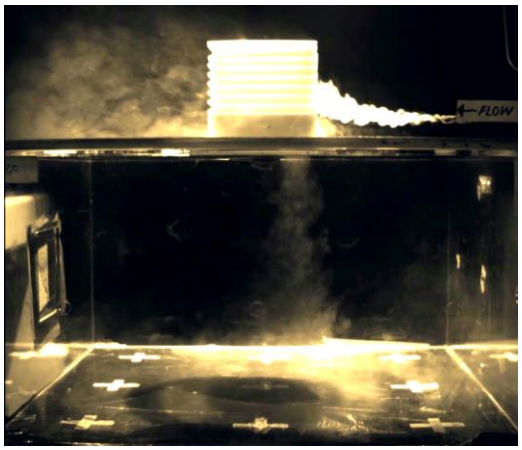

Video 1 Experimental flow visualisation inside the test room with the wind tower.

CFD streamline visualisation was carried out to demonstrate the top view of the passing flow through the wind tower model for various wind angles (Figure 17a), compared with wind tunnel smoke testing (Figure 17b and 17c). It was observed that at 0˚ angle, a large volume of the wind tower was used for extract purposes (three of the four quadrants). While the tower oriented at 45° into the prevailing wind had a larger area available to capture the wind. In this case, two windward quadrants were used for air flowing into the tower and two leeward quadrants for the air flowing out of the tower. A developing region of vortices was observed inside the windward quadrants at wind angles of 30˚ and 60˚ which reduced the induced operation of the wind tower. A similar flow pattern was observed in the experimental test. Therefore, the CFD flow simulation was considered validated.

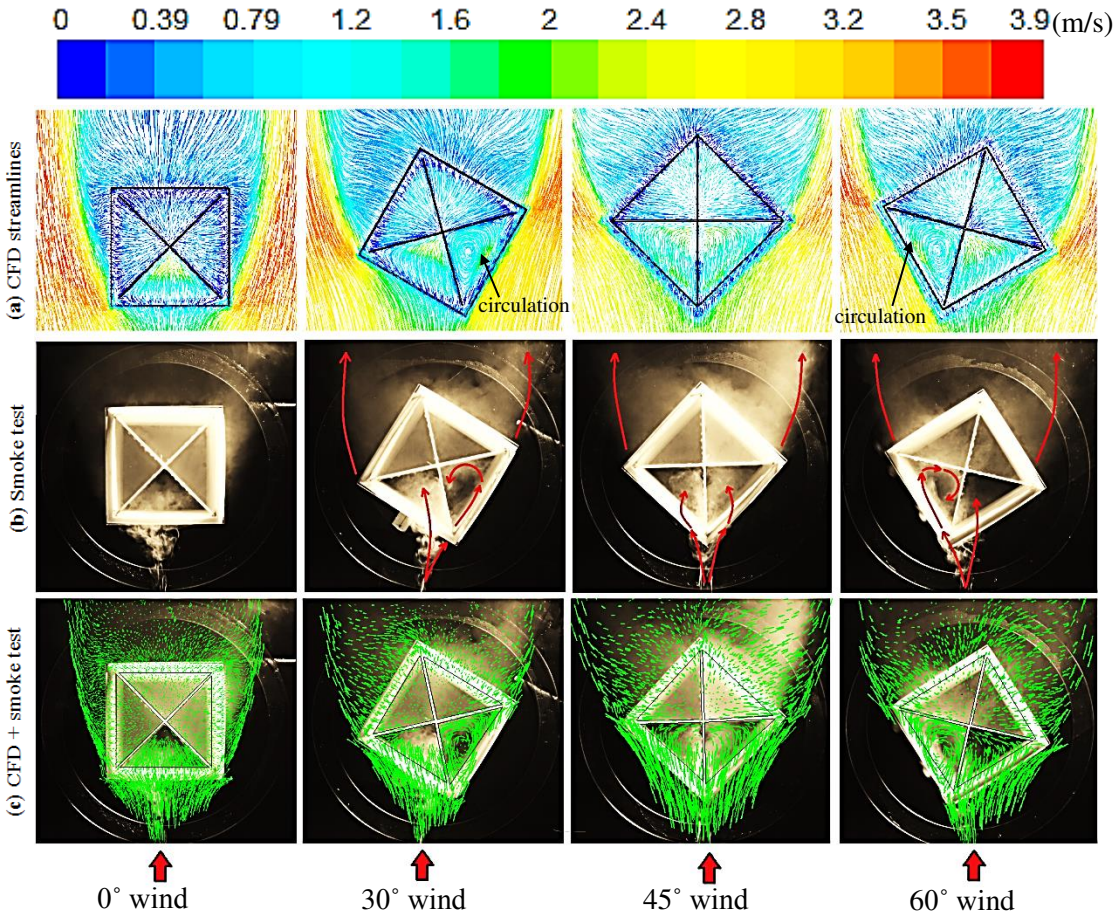

Figure 17 Visualised flow pattern inside the wind tower at various wind angles (top view): (a) CFD streamlines (b) experimental smoke testing (c) combined CFD vectors and smoke test results.

5. Conclusions

In this study, CFD and scaled wind tunnel experimentation have been used to investigate the natural ventilation performance of a commercial multi-directional wind tower. The CFD code was used to evaluate the airflow in and around the wind tower to the test room which represents a small classroom. A geometrical representation of the wind tunnel test set-up was recreated in the CFD simulation. Care was taken to generate a high-quality grid, specify consistent boundary conditions and compare the CFD simulation results with detailed wind tunnel measurements.

In order to have a valid comparison, the indoor and external airflow, supply rates, and pressure coefficients were calculated at points of the same positions used in the experimental test. A reduced-scale model (1:10) of the test room with a commercial multi-directional wind tower was constructed and placed in the closed-loop wind tunnel. Rigorous efforts were made to model the complex components of the wind tower. The tests were conducted at various

uniform wind speeds in the range of 0.5 to 5 m/s and various incidence angles, ranging from 0˚ to 90˚. The CFD simulations of indoor airflow distribution, ventilation rates, external airflow and surface pressures were generally in good agreement (0 – 20%) with the wind tunnel measurements.

Moreover, the smoke visualisation test showed the capability of CFD in replicating the air flow distribution inside the wind tower and also inside the test room model. The present work contributed to the extensive examination of a commercial multi-directional wind tower device.

Results have shown that multi-directional wind tower device was capable of supplying the recommended supply rates (10 L/s per occupant) for small classroom of 15 people at external wind speeds as low as 2 m/s for the considered test configuration. The CFD results for the indoor air pressure showed that the room was generally under negative pressure (external wind speed above 0.5 m/s) which indicated that less air was supplied to the room than exhausted which was the case for the multi-directional wind tower at 0˚ angle; there are three exhaust quadrants and only one supply quadrant.

The effect of different incident wind angles on the ventilation rates was also investigated. It was found that for a commercial multi-directional wind tower, the maximum efficiency was achieved at the angle of 45˚. At this wind angle, a net volumetric flow rate of 0.47 m^3/s (3 m/s external wind) was achieved through the combined supply quadrants, which was 32 % higher than the one at the angle of 0˚

Acknowledgement

The support by the University of Leeds (School of Civil Engineering) is gratefully acknowledged. The statements made herein are solely the responsibility of the authors.

Reference

[1] Ibn-Mohammed T, Greenough ,TRTaylor S, Ozawa-Meida L, Acquaye A, Integrating economic considerations with operational and embodied emissions into a decision support system for the optimal ranking of building retrofit options, Building and Environment, 2014, 72, 82-101.

[2] Deuble MP, de Dear RJ, Green occupants for green buildings: The missing link?, Building and Environment, 2012, 56, 21-27.

[3] Hughes BR and Ghani SA, A numerical investigation into the effect of Windvent louver external angle, Building and Environment, 2010, 45, 1025-1036.
[4] Liu S, Mak CM, Niu J**,** Numerical evaluation of louver configuration and ventilation strategies for the windcatcher system, Building and Environment, 2011, 46, 1600-1616.
[5] Montazeri H,Experimental and numerical study on natural ventilation performance of various multi-opening wind catchers, Building and Environment, 2011, 46, 370-378.
[6] Hughes BR, Calautit JK, Ghani SA, The Development of Commercial Wind Towers for Natural Ventilation: A Review, Applied Energy, 2012, 92, 606-627.
[7] Saadatian O, Haw LC, Sopian K, Sulaiman MY, Review of wind catcher technologies, Renewable and Sustainable Energy Reviews ,2012, 161477- 1495.
[8] Jones BM, Kirby R, Quantifying the performance of a top–down natural ventilation Windcatcher™, Building and Environment, 2009, 44, 1925-1934.
[9] Elmualim AA, Verification of design calculations of a wind catcher/tower natural ventilation system with performance testing in a real building, International journal of ventilation, 2006, 4, 393-404.
[10] Elmualim A, Dynamic modelling of a wind catcher/tower turret for natural ventilation Building Services Research and Technology, 2006, 27, 165-182.
[11] Hughes BR and Ghani SA, A numerical investigation into the effect of windvent dampers on operating conditions, Building and Environment, 2009, 44, 237– 248.
[12] Elmualim A, Effect of damper and heat source on wind catcher natural ventilation performance, Energy and Buildings, 2006, 38, 939–948.
[13] Chen Q, Srebric J, Simplified diffuser boundary conditions for numerical room airflow models, Final report for ASHRAE RP-1009, MIT, Cambridge; 2000.
[14] Su Y, Riffat S, Lin Y, Khan N, Experimental and CFD study of ventilation flow rate of a Monodraught™ windcatcher, Energy and Buildings, 2008, 40, 1110–1116.
[15] Calautit JK, Hughes BR, Ghani SA. A Numerical Investigation into the Feasibility of Integrating Green Building Technologies into Row Houses in the Middle East, Architectural Science Review, 2013, 56, 279-296.
[16] FLUENT Incorporated: FLUENT user guide [Online] 2006, available from: www1.ansys.com (access date December 1 2011)
[17] Building Bulletin 98: Briefing Framework for Secondary School Projects, [Online], 2004, available from: http://media.education.gov.uk

[18] Calautit JK, Chaudhry HN, Hughes BR, Ghani SA, Comparison between evaporative cooling and heat pipe assisted thermal loop for a commercial wind tower in hot and dry climatic conditions, Applied Energy, 2013, 101, 740-755.
[19] Chung T,Computational fluid dynamics,Cambridge University Press, 2002, 15-21.
[20] Hughes BR, Chaudhry HN, Calautit JK, Passive energy recovery from natural ventilation air streams, Applied Energy, 2013, 113, 127-140.
[21] Calautit JK, Hughes BR, Chaudhry HN, Ghani SA, CFD analysis of a heat transfer device integrated wind tower system for hot and dry climate. Applied Energy, 2013, 112, 576-59.
[22] Calautit JK, Hughes BR, Ghani SA, Numerical investigation of the integration of heat transfer devices into wind towers, Chemical Engineering Transactions, 2013, 34, 43-48.
[23] Calautit JK, Chaudhry HN, Hughes BR, Sim LF, A validated design methodology for a closed-loop subsonic wind tunnel, Journal of Wind Engineering and Industrial Aerodynamics, 2014, 125, 180-194.
[24] Cermak J, Isyumov N, Wind tunnel studies of buildings and structure, ASCE Publications, 1999.
[25] Cermak J, Applications of Fluid Mechanics to Wind Engineering, Journal of Fluids Engineering, 1975, 97, 9-38.
[26] Building Regulations 2000: Approved Document F1A: Means of Ventilation 2010, NBS: London.
[27] Zhang Z, Zhang, Zhai Z, Chen Q, Evaluation of Various Turbulence Models in Predicting Airflow and Turbulence in Enclosed Environments by CFD: Part 2—Comparison with Experimental Data from Literature, HVAC and R Research, 2007, 13, 871-886.
[28] Cook NJ, The designer's guide to wind loading of building structures: static structures pt.2 BRE Report, Butterworth-Heinemann Ltd, 1990.
[29] Lo LJ, Banks D, Novoselac A, Combined wind tunnel and CFD analysis for indoor airflow prediction of wind-driven cross ventilation, Building and Environment, 2013, 60, 12-23.
[30] Tecle A, Bitsuamlak GT, Jiru TE, Wind-driven natural ventilation in a low-rise building: A Boundary Layer Wind Tunnel study, Building and Environment, 2013, 59, 275-289.